JOURNAL OF
Bioactive and Compatible Polymers

Original Article

Journal of Bioactive and Compatible Polymers
2015, Vol. 30(5) 455–471

DOI: 10.1177/0883911515585183
jbc.sagepub.com
SAGE

Biocompatibility of Dead Sea Water and retinyl palmitate carrying poly(3-hydroxybutyrate-co-3-hydroxyvalerate) micro/nanoparticles designed for transdermal skin therapy

Gozde Eke[1,2,3], Felipe Goñi-de-Cerio[4], Blanca Suarez-Merino[4], Nesrin Hasirci[1,2,5] and Vasif Hasirci[1,2,6]

Abstract

In this study, novel drug carriers were developed for the treatment of skin conditions such as psoriasis, aging, or ultraviolet damage using micro/nanocapsules and micro/nanospheres of poly(3-hydroxybutyrate-co-3-hydroxyvalerate). The sizes of the particles were in the micron range and were loaded with retinyl palmitate and Dead Sea Water. In some tests, $MgCl_2$ was used as a substitute for Dead Sea Water for accurate determination of released ions of Dead Sea Water. Encapsulation efficiency and loading of water-soluble excipients Dead Sea Water and $MgCl_2$ were almost eight times lower than the hydrophobic compound retinyl palmitate. The particles were not cytotoxic as determined with the 3-(4,5-dimethylthiazol-2-yl)-2,5-diphenyltetrazolium bromide test using L929 mouse fibroblasts, BALB/3T3 mouse embryo fibroblasts, and HaCaT human keratinocytes. Ames test showed that the carriers were not genotoxic. The particles penetrated the membrane of human osteosarcoma cells Saos 2 and accumulated in their cytoplasm. No reactive oxygen species production could be detected which indicated low or

[1]Department of Micro and Nanotechnology, Middle East Technical University (METU), Ankara, Turkey
[2]BIOMATEN—Center of Excellence in Biomaterials and Tissue Engineering, Middle East Technical University (METU), Ankara, Turkey
[3]Department of Chemistry, Faculty of Arts and Sciences, Ahi Evran University, Kirsehir, Turkey
[4]GAIKER Technology Centre, Vizcaya, Spain
[5]Department of Chemistry, Middle East Technical University (METU), Ankara, Turkey
[6]Department of Biological Sciences, Middle East Technical University (METU), Ankara, Turkey

Corresponding author:
Vasif Hasirci, Department of Biological Sciences, Middle East Technical University (METU), Ankara 06800, Turkey.
Email: vhasirci@metu.edu.tr

no inflammatory response toward the particles. In the tests with intact human skin, 1.2% of the retinyl palmitate–loaded poly(3-hydroxybutyrate-co-3-hydroxyvalerate) particles penetrated into the human skin, but when the skin was without stratum corneum and increased to 6.9%. In conclusion, these carriers have shown a significant potential as topical drug delivery systems in the personalized treatment of skin diseases because their contents could be modified according to a patient's needs and several drugs could be loaded in one type of microparticle, or several populations, each carrying a different drug, can be used in the treatment.

Keywords
Drug delivery systems, biopolymers, microparticles, nanoparticles, skin diseases, personalized treatment.

Introduction

Controlled drug delivery systems are becoming increasingly important with the contribution of nanotechnology. In the case of topical applications, use of micro- and nanoparticles as drug carriers is a very promising method since the greatest limitation is the highly impermeable outermost layer of the skin, stratum corneum, and micro- and nano-sized particles have the potential to carry drugs across to it. Encapsulation of drugs in nanoparticles, as opposed to classical topical application of creams or emulsions, allows the particles to diffuse into the hair follicles and release the drug in the deeper layers of the skin. Although there are many drug delivery routes such as subcutaneous, oral, intramuscular, intravenous, and topical, topical administrations are advantageous because they have no systemic toxicity and the route to the target site is short.[1] They are preferable because of their high efficacy in localized treatments, low cost, and maximum bioavailability at the target site.[2] One of the greatest challenges that need to be overcome is the difficulty in the permeation of the drug through the skin because of the tightly organized stratum corneum and the underlying skin layers.[3] Drugs have to be absorbed at an adequate rate to achieve and maintain uniform, systemic, or local therapeutic levels.[4] If drug is applied in free form such as a cream, it can be washed away before complete penetration. In order to prolong the bioavailability and enhance permeability, the most suitable delivery systems are the nanoparticulate carriers.

Drugs for transdermal delivery have three routes to cross the epidermis: intercellular (paracellular, in between the corneocytes), intracellular (transcellular, across the corneocytes), and through the appendageal shunt (transappendageal).[5] Intracellular path is longer than stratum corneum thickness; therefore, the most common penetration route is the intercellular. Micro- and nanoparticles prefer the appendageal route. Hair follicles occupy only about 0.1% of the total skin surface area; however, below the skin surface, epidermis invaginates into the dermis, and this increases both the absorption area and the depth penetrated.[6]

Nanocarriers have three important properties as delivery systems: (1) high rate of release due to the high surface-to-volume ratio, (2) extravasation leading to release of the drugs in regions with compromised vasculature, and (3) ease of transportation across biological membranes including the blood–brain barrier (BBB).[7–10]

The materials used to encapsulate drugs can be ceramics,[11] inorganic materials,[12] polymeric,[13] or lipoid particles.[14] Nanoparticles were used in the delivery of DNA,[15] antitumor drugs,[16] and in the transfer of drugs that need to cross the BBB.[17] Skin damaged by aging was shown to be repaired by using nanoparticles loaded with vitamin A derivatives[18] or by using a cream containing retinoid derivatives.[19] Penetration of polyethylene glycol (PEG)-coated CdSe quantum dots in abraded mouse skin was reported.[20]

Biodegradable polymers are preferable as drug carriers, and the widely used Food and Drug Administration (FDA)-approved polymers are poly(lactic acid) (PLA), poly(glycolic acid) (PGA), poly(lactide-co-glycolide) (PLGA), poly(ε-caprolactone) (PCL), alginate and chitosan,[21] and their blends. Poly(hydroxyalkanoates) (PHAs) constitute another important polymer family which is produced by bacteria. PHA molecules with complex chemical structures can be produced starting from simple sugars.[10,22] The most widely studied PHAs are poly(3-hydroxybutyrate) (P3HB) and poly(3-hydroxybutyrate-co-3-hydroxyvalerate) (PHBV). Their biological origin, biocompatibility, biodegradability by natural mechanisms, and our capability to tailor their properties to our needs by changing the hydroxyvalerate (HV) content of the polymer make PHBV more appealing than synthetic polylactides and polyglycolides.[23,24] Delivery of conventional drugs, recombinant proteins, nucleotides, and growth factors via micro- and nanoparticles of PHBV is reported in the literature.[22,25–27]

In this study, two main bioactive agents were used. One is Dead Sea Water (DSW) which is basically a salt solution with quite complex composition. Traditionally, therapeutic baths, like those near the Dead Sea area, are used as a treatment site for skin diseases such as psoriasis, atopic dermatitis, and ultraviolet (UV)-damaged skin.[28] It was also reported that the mud from the Dead Sea accelerates wound healing when applied on BALB/c mice; enhanced granulation, wound contraction, epithelialization, angiogenesis, and collagen deposition were the indicators of this healing. This was explained to be a result of high mineral and trace element content of the water that possibly acts as an anti-inflammatory and antioxidant which enhance cell proliferation, migration, and fibroblast cellular activity.[29]

The other bioactive agent used was retinyl palmitate (RP). RP was selected because it is the most stable form of vitamin A and has an important role in cell differentiation and in the prevention of carcinogenesis.[30] RP is also used in pharmaceutical preparations formulated to serve as an anti-aging agent.[31]

In this study, PHBV micro/nanoparticles (MNPs) were prepared to serve as transdermal drug carriers. RP and DSW were tested as model drugs. The particles were characterized by their encapsulation efficiency (EE), in situ drug release kinetics, and in vitro cell penetration, cytotoxicity, and genotoxicity. Apoptotic trends were studied by measuring the levels of reactive oxygen species (ROS) and cytokine produced in response to exposure of the cells to the particles. Penetration of drugs was studied using human skin. Although studies involving PHBV nanoparticles as drug carriers were reported earlier,[10,25,26] the use of RP and DSW carrying PHBV nanoparticles for transdermal skin therapy is being reported for the first time. In a similar study, RP was released from a synthetic polyester PLGA nanospheres;[27] however, in addition to the difference in the carrier chemistry, we used both nanospheres and nanocapsules. In our study, data on DSW entrapment and its release behavior as well as hemocompatibility were included adding further insight to the study. Qualitative and quantitative uptake of the nanoparticles by the cells, in vitro and the ex vivo penetration of RP released from the nanoparticles through intact or abraded human skin patches were also investigated. The biocompatibility of the particles was investigated in detail by carrying out cyto- and genotoxicity tests towards the particles with 3-(4,5-dimethylthiazol-2-yl)-2,5-diphenyltetrazolium bromide (MTT) and Ames tests, respectively. Production of ROS was shown to reveal very low inflammatory response.

Materials and methods

Materials

PHBV (HV content 5%, w/w), RP, and MTT kit were from Sigma–Aldrich (USA). Polyvinyl alcohol (PVA) and magnesium chloride (MgCl2) were from Fluka (USA). DSW was a kind gift of

Dead Sea Laboratories Ltd (Israel). Chloride-specific electrode and ion meter were from Cole-Parmer Instrument Company (USA), and oxidant-sensitive fluorescent probe, 2′,7′-dichlorofluorescein diacetate (H_2DCFDA), was from Invitrogen (USA). Peripheral blood samples were collected from healthy consenting adults by venipuncture at the Middle East Technical University (METU) Medical Center. Blood samples were collected in ethylenediaminetetraacetic acid (EDTA)-containing tubes and used immediately after collection for hemolytic activity tests. Dulbecco's Modified Eagle Medium (DMEM; high glucose), RPMI-1640 medium, fetal bovine serum (FBS), and penicillin/streptomycin were all purchased from HyClone (USA). Human osteosarcoma cell line (Saos 2) was from American Type Culture Collection (ATCC; No. CCL-1); L929 cell line was from the Foot-and-Mouth Disease Institute (Ankara, Turkey); BALB/3T3 mouse fibroblasts and HaCaT human keratinocyte cells were from ECACC (UK) and CLS (Germany), respectively.

Methods

Preparation of RP-loaded micro/nanospheres. RP-loaded micro/nanospheres (MNS_RP) were prepared with the oil-in-water (o/w) technique. For this purpose, RP was added into 1.2 mL of solution of PHBV in dichloromethane (DCM; 10%, w/v) (PHBV:RP 4:1 w/w). This solution was added into an aqueous solution of PVA (4 mL, 4% w/v), sonicated in an ice bath; further dilution was made by adding PVA solution (100 mL, 0.3% w/v), stirred overnight at room temperature to remove the solvent, and centrifuged (12,500 r/min, 10 min). The precipitate was washed twice with distilled water (dH_2O), resuspended in distilled water, and then lyophilized. The Nile Red–loaded micro/nanospheres (MNS_NR) were prepared similarly by adding the dye instead of RP.

Preparation of DSW- or $MgCl_2$-loaded micro/nanocapsules. DSW- or $MgCl_2$-loaded micro/nanocapsules were prepared by using the water-in-oil-in-water (w/o/w) solvent evaporation technique. An emulsion was formed by adding DSW (200 µL) or $MgCl_2$ solution (200 µL, 1 g/mL in dH_2O) into PHBV solution (1.2 mL, 10%, w/v in DCM), sonicated for 15 s, added into an aqueous solution of PVA (4 mL, 4%, w/v). The rest of the process was similar to MNS_RP preparation.

Characterization

Particle topography and size distribution analyses by scanning electron microscopy. Aqueous suspension of MNPs was added onto carbon tapes attached to scanning electron microscope (SEM) stubs, dried at room temperature, and then sputter coated with Au-Pd before examining with SEM (Quanta 400F Field Emission SEM, The Netherlands). The sizes were measured with Image J software, NIH (USA), and surface topography was examined from the images.

RP loading and encapsulation efficiency. The concentration of RP entrapped in PHBV particles (10 mg) was determined after dissolving the particles in DCM (3 mL) and measuring the absorbance at 325 nm with UV spectrophotometer.

For confirmation of the accuracy of the analysis, the amount of RP was also determined with high-performance liquid chromatography (HPLC) using an ODS 3 column with methylene chloride in methanol (60% v/v) as the mobile phase and a flow rate of 1 mL/min with fluorescence detector. RP was determined at λ_{ex}: 325 nm and λ_{em}: 470 nm (n = 2).

DSW and $MgCl_2$ loading and encapsulation efficiency. DSW has a very high chloride ion (Cl^-) content (350 mg/mL); therefore, calculations of the EE of DSW or $MgCl_2$ were based on determination of Cl^-. For this purpose, chloride was extracted by dissolving the loaded MNCs (20 mg) in DCM

(6 mL) and adding ultrapure water (2 mL). After phase separation, the aqueous phase containing the ions was removed and the Cl^- content was determined with a chloride-specific electrode and an ion meter (Cole-Parmer Instrument Company). Each test was run in triplicate (n = 3).

The values for loading (%) and EE (%) were calculated by using the following equations

$$\text{Loading (\%)} = [\text{Amount of encapsulated } MgCl_2 \text{ (mg)/Total amount of MNC (mg)}] \times 100$$

$$\text{EE (\%)} = [\text{Amount of encapsulated } MgCl_2 \text{ (mg)/Input amount of } MgCl_2 \text{ (mg)}] \times 100$$

In situ release of DSW and $MgCl_2$ from micro/nanocapsules. The particles were suspended in ultrapure water (5 mL, 10 mg/mL) and placed in a shaking incubator (Innova 4000; New Brunswick Scientific, USA) at 37°C. This suspension was agitated for a week. At various time points (1 h, 3 h, 6 h, 12 h, 2 days, and 7 days), tubes were centrifuged, supernatant was removed, and the amount of Cl^- ions released was determined with the chloride-specific electrode. The data was presented as "released $MgCl_2$ and DSW concentration vs time" and treated according to Higuchi equation ($M_t/M\infty$ vs $t^{1/2}$).

Determination of hemolytic activity of the micro/nanoparticles. Hemolytic activity tests were made in accordance with a modified American Society for Testing and Materials (ASTM) procedure.[32] Human peripheral blood was collected from volunteers in EDTA-containing tubes, centrifuged (20°C, 3400 r/min, 15 min), and the red blood cells (RBCs) in the pellet were resuspended in phosphate-buffered saline (PBS) (20 mL). This suspension (1 mL) was added into solutions having different amounts of particles (0.1–1 mg/mL), incubated at 37°C for 1 h, and centrifuged (1500 r/min, 20 min). Then 200 µL of the supernatants was transferred to 96-well plates (n = 3). Absorbance at 540 nm was measured. As negative control, RBC solution without nanoparticles was used. As positive control, complete hemolysis was achieved by diluting the RBC suspension with ultrapure water (1:10) and then incubating at 37°C for 1 h.

In vitro studies

Cell cultures. In in vitro studies, L929 and BALB/3T3 mouse fibroblasts (ECACC 86110401) and HaCaT human keratinocytes (CLS 300493) were used. All cell lines were grown as a monolayer in tissue culture flasks in CO_2 incubator at 37°C and after 70% confluence subcultured in new culture flasks. At least 24 h before the performance of the cytotoxicity assays, the cells were detached using trypsin–EDTA solution and counted. To 96-well plates for MTT and inflammation tests, 200 µL of cell suspension (80,000 cells/mL) was added, and 1 mL of cell suspension was added to 24-well plates for ROS production studies. Plates were incubated (37°C, 5% CO_2) for 24 h. Various amounts of particles were also incubated with these cells in the culture media for 24 h or 7 days to study the influence of particle concentration on cell proliferation.

Cell viability. The particles were incubated with L929 cells (20,000 cells/mL) for 24 h (37°C, 5% CO_2). After the removal of the medium, the wells were washed twice with sterile PBS. MTT solution (1 mL) was added into each well and incubated for 3 h. Then MTT solution was replaced with acidified isopropanol (1 mL) to dissolve the formazan crystals formed by the cells. To 96-well plates, 200 µL of this solution was added, and absorbances were measured at 550 nm by UV spectrophotometer on Days 3 and 7 (n = 3).

For the determination of influence of particle concentration on cell proliferation, cells were treated with unloaded and loaded particles using different concentrations (0.02–2.5 mg/mL) for 24 h. After incubation, cells were washed twice with PBS, and the procedure given in the previous

section was followed. The corresponding "standard error mean" was calculated for three independent experiments and six replicates for each experimental point.

Determination of cytokines. Cytokine (tumor necrosis factor α (TNFα), interleukin (IL)-1β, IL-6, IL-8, IL-10) concentrations were determined by ELISA assay (BD OptEIA, USA) according to the manufacturer's recommendations. HaCaT and BALB/3T3 cells were treated with MNPs (0.1 and 0.5 mg/mL) for 24 h. Tert-butyl hydroperoxide solution (200 μM; Sigma, USA) was used as the positive control. After incubation, cell medium was diluted 4-fold in the assay diluent and incubated with conjugated cytokine antibody. Following multiple plate wash cycles, the substrate tetramethylbenzidine was added, and the absorbances were measured at 450 nm. The results were analyzed to determine cytokine levels using a four-parameter fit of the standard curve. Three independent experiments and at least three replicates for each experimental point were done.

Production of ROS. Intracellular ROS concentrations were determined by using the oxidant-sensitive fluorescent probe, H_2DCFDA (Invitrogen). Cells (10,000 cells/100 μL) were exposed to MNPs (0.1 and 0.5 mg/mL) for 24 h prior to staining. Cells stained by incubating with H_2DCFDA (10 μM) at 37°C for 30 min were washed with PBS, and cell fluorescence at 4°C was determined by flow cytometry (Cytomics FC500-MCL). Three independent experiments and at least three replicates for each experimental point were carried out. HaCaT and BALB/3T3 cell lines were treated with tert-butyl hydroperoxide (200 μM) as the positive control.

Genotoxicity. The Ames test measures the potential of a test compound to achieve a back mutation that causes the histidine synthesizing gene of *Salmonella typhimurium* to regain its function and allow it to grow in a histidine-free medium (Moltox, USA). The reverse mutation test uses five histidine auxotrophic strains of *S. typhimurium*, to detect specific mutations such as substitution, addition, or deletion of one or several base pairs. In this study, five strains of *S. typhimurium,* namely, TA98, TA100, TA1535, TA1537, and TA102 were used according to Organization for Economic Co-operation and Development (OECD) Guideline 471. Two sets of experiments were carried out with and without metabolic system activation (AroclorTM 1254–induced rat liver S9, prepared from adult Sprague–Dawley rats). The plates were also examined visually for inhibition of growth in the bacterial lawn and no inhibition was observed under the conditions of the study. Briefly, cultures were prepared on nutrient broth (Oxoid No. 2) in a shaking water bath at 37°C. Positive reference reagents were included in the experiment as recommended by OECD Guideline 471. Assays were performed with 500 μL of the S9 mixture of aroclor 1254–induced rat liver homogenate. The experiments were carried out in triplicates. Five-fold dilutions of MNS, MNS_RP, and DSW-loaded micro/nanocapsules (MNC_DSW) were used starting from 5 mg/plate. Tubes were incubated for 60 min at 37°C and 90 r/min in a shaking water bath. Then, soft agar (2.0 mL) was added along with histidine (0.05 mM), vortexed, and plated on Vogel–Bonner plates Maron and Ames (BN, 1983). Histidine revertants (His^+) were counted in a Fisher Colony Counter after incubation for 48 h at 37°C.

Detection of particle uptake by the cells. Interactions of MNS_NR with the cells were studied with Saos 2 cells. Incubation of cells and addition of the particles to the cells were similar to the procedure given previously.[10] Briefly, after 24 h of incubation in RPMI medium supplemented with 10% FBS and 1% penicillin/streptomycin (100 units), Saos 2 cells were seeded into a six-well plate containing MNS_NR (0.5 mg/mL). After 24 h of incubation, cells were fixed with paraformaldehyde, stained with Draq5 and fluorescein isothiocyanate (FITC)-conjugated phalloidin for detection

of nucleus and the cytoskeleton, respectively, and were examined with confocal laser scanning microscopy (CLSM; Leica DM2500, Germany).

In order to quantify particle uptake by the cells, Saos 2 cells (100,000) were seeded into a six-well plate containing MNS_NR (0.5 mg/mL). After 24 h incubation, cells were washed with PBS to remove excess nanoparticles. One milliliter of Isotonic Cell Lysis Buffer (10 mM Tris 7.5, 2 mM $MgCl_2$, 3 mM $CaCl_2$, 0.3 M sucrose) and Triton X-100 (1 mL/well) was added into the wells, kept on ice for 15 min, and then the swollen cells were mechanically removed from the plates. Cell suspension was centrifuged, supernatant and acetone were mixed in a 1:1 ratio to dissolve the Nile Red, and its fluorescence intensity was measured (λ_{ex}: 552 nm, λ_{em}: 636 nm) using a spectrofluorometer (Spectramax M2, Molecular Devices, USA). The experiments were carried out in triplicates (n = 3). A calibration curve was prepared using Nile Red dissolved in acetone-isotonic cell lysis buffer and Triton X-100.

Studies on penetration through human skin. Skin samples were obtained from a 42-year-old, healthy donor admitted for elective breast surgery (upon her consent and with METU-Animal Experiments Local Ethics Committee approval). Skin samples (2×2 cm^2) were inserted into cell crown holders in 12-well plates exposing the epidermis to air while the dermis is in PBS. Stratum corneum of some samples was mechanically removed to study its inhibitory effect on penetration. MNS_RP (0.5 mg) were placed on each skin sample. After a 24-h incubation period, the particles were gently removed from the skin surface, and the skin samples were put in chloroform (10 mL) and stirred for 72 h for skin and nanoparticle destruction. The RP that dissolved out was determined with UV–visible (Vis) spectrophotometry (λ_{max}: 326 nm) (n = 5) using a calibration curve.

Statistical analyses. The results were contrasted with a Levene test to confirm the homogeneity of variance between the different treatments and Kolmogorov–Smirnoff test for normality. One-factor analysis of variance (ANOVA) with Bonferroni–Dunn's correction was performed to assess differences in DCFDA, cytokine release labeling as a function of group. Comparison between parameters was performed by two-factor ANOVA for repeated measurements as a function of groups. The value of $p \leqslant 0.05$ was considered significant.

Results and discussion

Topography, size, and size distribution of MNPs

PHBV particles were produced according to the procedures used in our previous studies conducted with similar polymers,[10,22] and the SEM micrographs of unloaded as well as RP-loaded spheres (MNS_RP) and DSW-loaded capsules (MNC_DSW) were similar and had smooth surfaces (Figure 1). The average diameters of the particles were in the range 4.0–6.1 μm (Table 1). Loading did not change the size or the appearance for micro/nanocapsules while the sizes of micro/nanospheres increased. This shows that when the ionic chemical (DSW) is loaded in the central cavity of the capsule, the size does not change, but when the hydrophobic compound RP is loaded in the bulk of the sphere, the size increases. Similar observations, such as an increase in the size of PLGA particles, from 508 ± 127 to 531 ± 73.33 nm, after loading of a vitamin A derivative, were reported.[33] In our study, approximately 45% of the particles were smaller than 3 μm in all formulations and this range is suitable for transdermal penetration. However, the size should be smaller than 500 nm for penetration into the cells, and 25% of our particles were in this range indicating that a large fraction of the particles could penetrate the skin and a reasonable amount is suitable for endocytosis.[10]

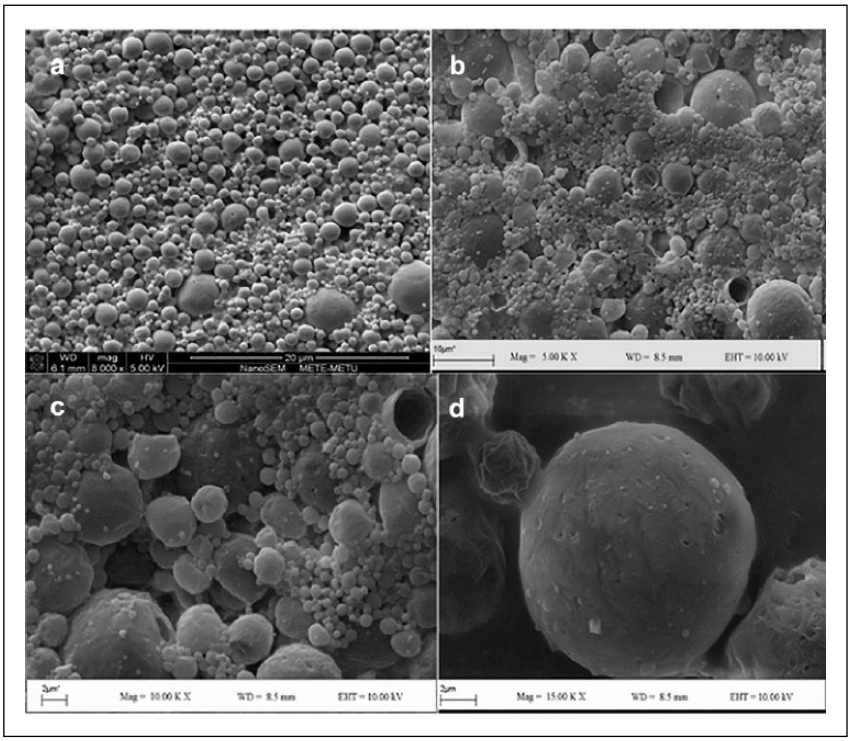

Figure 1. SEM images of bioactive agent–loaded PHBV particles: (a) RP-loaded spheres (MNS_RP). Magnification: 8000×. (b) DSW-loaded capsules (MNC_DSW). Magnification: 5000×. (c) General appearance showing size distribution unloaded MNC. Wall thicknesses were calculated using the images of the broken capsules. Magnification: 10,000×. (d) Close up of the largest capsule; it is spherical in shape and has a smooth surface. Magnification: 15,000×. Loading of the bioactive agents did not affect the smoothness and roundness of the particles. Also, capsule and sphere forms are very similar to each other in terms of average size and appearance.

Encapsulation of RP in MNS

EE of RP in PHBV spheres determined using two different methods, HPLC (with fluorescence detector) and UV–Vis spectrophotometry, were very similar (ca. 8% and 8.5%) (Table 1). The loading process of hydrophobic drugs in hydrophobic particles is reported to involve hydrophobic interactions between the drug and the polymeric chains.[34] In the literature, 3.4% RP loading in poly(L-lactic acid) (PLLA) nanoparticles, and 1% and 0.94% retinoic acid loading in PLGA and PHBV particles, respectively, were reported.[33,35] The results obtained in this study are not high but are comparable to those in the literature and were used in the following studies.

Encapsulation of $MgCl_2$ and DSW in MNC

DSW is a complex mixture of ions, and determination of separate ions is not possible so its concentration was calculated using the electrical conductivity of the medium. Determination of individual ions was not possible due to possible interference by other ions. Therefore, when a specific ion was to be determined, a chloride detector was used. In such cases, $MgCl_2$ was loaded instead of DSW. Therefore, $MgCl_2$ with chloride ion concentration equal to that of DSW was loaded into

Table 1. Size of PHBV MNPs, and encapsulation efficiency and loading of bioactive agents in MNPs.

MNP type	Bioactive agent	Detection method	Average size	EE (%)	Loading (%)
MNS	Unloaded	–	4.0 ± 1.6 µm	–	–
MNC	Unloaded	–	4.3 ± 2.8 µm (wall thicknesses of 105 ± 31 nm)	–	–
MNS	RP	HPLC, fluorescence detector; λ_{ex}: 325 nm, λ_{em}: 470 nm	6.1 ± 2.4 µm	8.0 ± 0.0	1.4 ± 0.1
MNS	RP	UV–Vis spectrophotometry; $\lambda_{max:}$ 326 nm	6.1 ± 2.4 µm	8.5 ± 0.2	1.5 ± 0.1
MNC	$MgCl_2$	Chloride-specific electrode and ion meter	4.6 ± 2.4 µm	1.7 ± 0.2	1.0 ± 0.1
MNC	DSW	Chloride-specific electrode and ion meter	4.3 ± 1.2 µm	1.1 ± 0.1	0.9 ± 0.1

PHBV: poly(3-hydroxybutyrate-co-3-hydroxyvalerate); MNP: micronanoparticle; MNS: micronanosphere; MNC: micronanocapsule; EE: encapsulation efficiency; RP: retinyl palmitate; HPLC: high-performance liquid chromatography; UV: ultraviolet; Vis: visible; DSW: Dead Sea Water.

the MNC. EEs of DSW and $MgCl_2$ were calculated as 1.1% and 1.7%, respectively (Table 1). Low values such as 1.29% for metformin hydrochloride in PHBV8[36] and 1.5% for carboxyfluorescein in PHBV14 nanocapsules were reported.[37] These low values could be explained by the leakage of the ions during MNC preparation steps due to their high solubility.

Release kinetics of $MgCl_2$ and DSW

The release behavior of $MgCl_2$ and DSW was analyzed by applying first-order and second-order kinetics equations and Higuchi equation ($M_t/M\infty = kt^{1/2}$, M_t = amount of released drug at certain time (t), $M\infty$ = the maximum release at infinite time, and k = release rate constant). The results are presented in Figure 2 and Table 2. The best fit was obtained with the Higuchi model (Figure 2, inset) (r^2 values were higher than 0.9 for both $MgCl_2$ and DSW). Most of the content was released in the first 24 h and the release was almost complete in 48 h. This burst release rate is high, but it is acceptable since a high drug concentration in the beginning of treatment saturates the system with the burst and later low rate of release maintains the drug level.

Hemolytic activity of PHBV MNS and MNC

In earlier studies, no adverse effects of PHBV MNPs were reported in in vitro and in vivo tests,[10,22,38] and they were not hemolytic (hemolysis <5%).[39,40] According to the ISO/TR 7405-1984(f), a sample is considered hemolytic only when the hemolytic activity is above 5%. In our study, the hemolysis levels were very low (0.8% for MNS, 1.0% for MNC_DSW, and 1.4% for MNS_RP). It can, therefore, be safely stated that the PHBV particles tested in this study were not hemolytic. Besides, the erythrocytes examined with light microscopy did not reveal any morphological changes supporting the compatibility of the particles with the erythrocytes.

In vitro studies

Influence of bioactive agent–loaded particles on the proliferation of L929 fibroblasts. MTT test was used to determine the effects of particles on the viability and proliferation of L929 fibroblasts. Both free

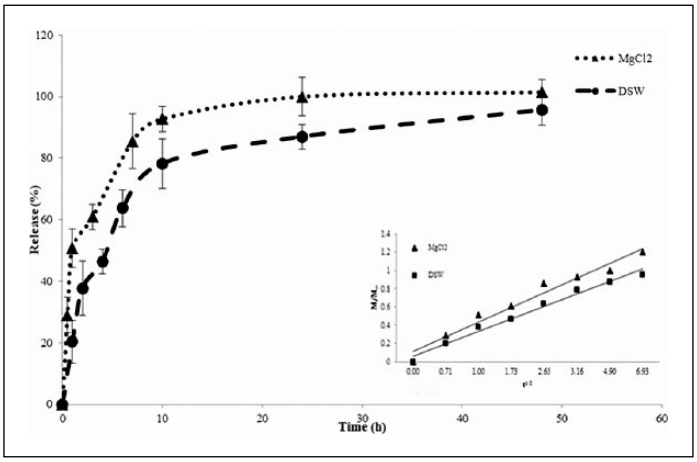

Figure 2. Release of $MgCl_2$ and DSW from PHBV MNC. Inset represents the data plotted according to Higuchi model. Quantification was made by measuring the chloride ion concentration in ultrapure water at 37°C (n = 3).

Table 2. Release behavior of $MgCl_2$ and DSW from PHBV MNC.

Samples	Release models, rate constant (k) and r^2 values					
	Zero order		First order		Higuchi	
	k_o	r^2	k_1	r^2	k_H	r^2
$MgCl_2$	0.0053	0.4753	0.0174	0.4242	0.1602	0.9678
DSW	0.0067	0.6105	0.0229	0.5005	0.1360	0.9851

DSW: Dead Sea Water; $MgCl_2$: Magnesium chloride; PHBV: poly(3-hydroxybutyrate-co-3-hydroxyvalerate); MNC: Micro/nanocapsule.

DSW and RP suppressed L929 proliferation by about 50% in comparison to the control (Figure 3). It is known that RP is a skin irritant and has a number of side effects such as causing skin dryness, wounds and toxicity.[18,41] Thus, the decrease in cell proliferation by free RP was expected. Similarly, suppression of proliferation by DSW was expected because of its high salt concentration. Upon entrapment into particles, however, the adverse effects of RP and DSW were significantly decreased; DSW became completely nontoxic. The masking of the adverse effects is probably because of the decrease in their bioavailability due to release process.

Influence of particle concentration on cell proliferation. In the literature, there is no consensus on the toxic effect of the nanoparticles because of the difference in the methods and the cell lines used in testing. The most widely used test is the MTT viability assay that basically involves the determination of the activity of a mitochondrial enzyme.[42,43] In this study, cell lines were treated for 24 h with 10 different particle concentrations (0.02–2.50 mg/mL). In all cases, MTT test results showed that proliferation of HaCaT and BALB/3T3 cells were not affected by the presence of the particles at any concentration (Figure 4(a) and (b)). The lethal concentration that produces 20% cell death (LC20) for unloaded spheres in 3T3 and HaCaT cell lines was 0.61 ± 0.16 and 0.57 ± 0.09 mg/mL,

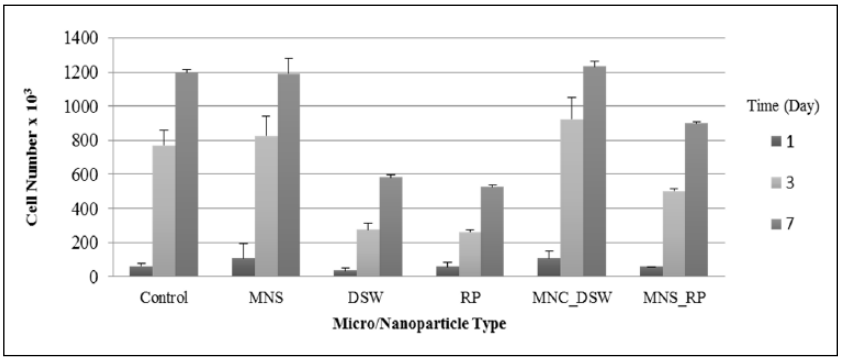

Figure 3. Results of MTT tests showing the effect of bioactive agent–loaded MNP on L929 cell proliferation. Control has no MNP and no bioactive agent. Test duration: 7 days (n = 3).

respectively. For the same cells, LC20 values for MNS_RP were 0.68 ± 0.08 and 0.51 ± 0.11, and for MNC_DSW were 0.56 ± 0.1 and 0.60 ± 0.05, respectively. LC50 and LC80 values (50% and 80% of cell death, respectively) were also calculated, and these values obtained with both cell lines were higher than 0.8 and 1.5 mg/mL, respectively. The results indicate that the toxicity of nanoparticles is concentration dependent and RP and DSW are not specifically implicated in cytotoxicity.

Assessment of inflammation. In this study, we have taken into account that MNPs could interfere with dyes and their products in viability assays by absorbing the constituents from the cell medium.[44,45] On the other hand, although no cell death may be apparent after nanoparticle exposure, changes in cellular function may occur. Therefore, sub-lethal cellular changes have also been assessed after particle exposure on the cell membrane asymmetry, ROS production, mutagenicity, and cytokine release to ensure that valid conclusions are drawn. Inflammation is a possible adverse effect upon exposure of cells to nanoparticles. In this study, pro-inflammatory cytokines (IL-1β, IL-6, IL-8, and TNFα) were analyzed along with the IL-10 which belongs to the anti-inflammatory group.[46,47] Following the toxicity results, particle concentrations of 0.1 and 0.5 mg/mL were chosen to perform more sensitive inflammation studies focused on early cellular damage such as ROS production and cytokine release. In these particles, the amounts of RP in MNS_RP were 1.5 and 7.5 ng/mL, and DSW in MNC_DSW were 0.3 and 1.5 ng/mL, respectively.

The results of inflammation experiments showed that cytokine levels were similar after 24 h in cells exposed to all nanoparticles (Table 3). HaCaT cell lines treated with 200 μM t-butyl hydroperoxide serum showed a significant increase in TNFα, IL-6, IL-8, and IL-10 secretion in comparison to untreated HaCaT cultures. HaCaT cells treated with MNS, MNS_RP, and MNC_DSW (0.1 and 0.5 mg/mL) showed an increase in IL-8 ($p < 0.05$) production in comparison to control cultures. However, levels of TNFα, IL-6, and IL-10 were either decreased or there was no significant change compared to control. For BALB/3T3 cell line, an increase in all cytokine expressions was observed after t-butyl hydroperoxide treatment. IL-10 levels were significantly increased ($p < 0.05$) in MNS_RP- and MNC_DSW-treated cultures at both particle concentrations, compared to BALB/3T3-untreated cultures.

In vitro biological evaluations have shown that the cytocompatibility of all the particles was high. The absence of a stronger cellular inflammatory response in keratinocytes and fibroblast cell lines, despite an increased IL-8 content in HaCaT, represents a low inflammatory response during incubation with both nanosystems. Likewise, the significant release of IL-10, which has the capacity to downregulate the production of inflammatory cytokines and chemokines[48] was shown in fibroblast cell

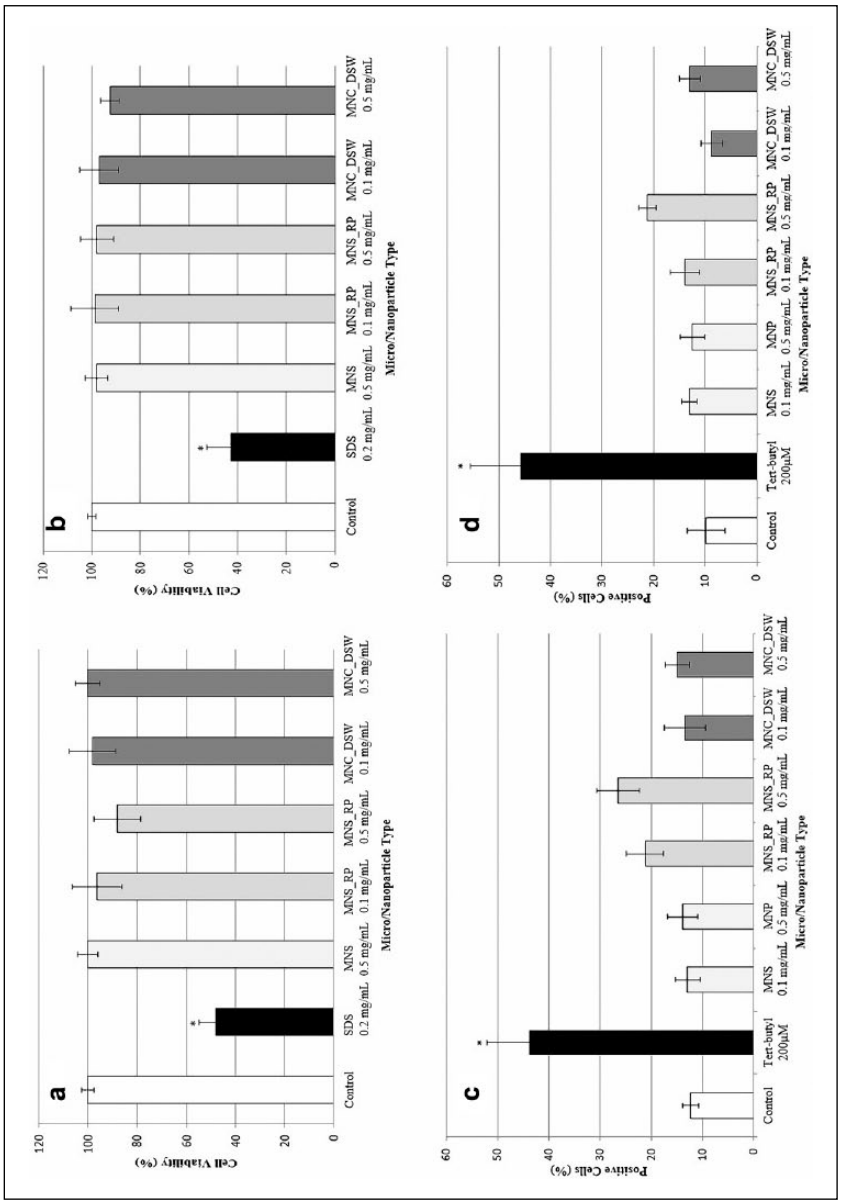

Figure 4. The influence of MNP-loaded RP and DSW on viability of (a) HaCaT and (b) BALB/3T3 cell lines. Values are expressed as the mean of cell viability % ± SD as determined with MTT assay. Generation of ROS in (c) HaCaT and (d) BALB/3T3 cell lines by the MNP-carrying RP and DSW. Measurement is based on the cell fraction stained with DCFDA. Values are expressed as the mean of positive cells ± SD. One-factor analysis of variance (ANOVA) was performed. Test duration: 24 h.
SDS: sodium dodecylsulfate.
*$p < 0.05$ with respect to control culture.

Table 3. Production of inflammatory cytokines by HaCaT and BALB/3T3 cells in the presence of micro/nanoparticles.

Cell type	Control	Tert-butyl (200 µM)	MNS (0.5 mg/mL)	MNS_RP (0.1 mg/mL)	MNS_RP (0.5 mg/mL)	MNC_DSW (0.1 mg/mL)	MNC_DSW (0.5 mg/mL)
HaCaT							
TNFα	10.21 ± 2.23	25.08 ± 4.26*	8.69 ± 1.69	11.86 ± 2.95	11.02 ± 1.98	10.47 ± 2.46	10.75 ± 3.18
IL-1β	5.74 ± 3.58	11.31 ± 2.05	0.98 ± 0.23	8.09 ± 3.25	6.76 ± 1.54	8.96 ± 2.78	6.4 ± 1.04
IL-6	10.29 ± 2.84	87.03 ± 7.94*	4.41 ± 1.23	4.04 ± 3.16	9.11 ± 2.23	5.64 ± 3.52	7.84 ± 2.91
IL-8	17.34 ± 3.69	190.37 ± 8.95*	29.34 ± 4.7*	32.98 ± 4.51*	44.88 ± 5.8*	29.23 ± 3.92*	31.14 ± 4.28*
IL-10	12.48 ± 1.85	106.01 ± 7.23*	6.64 ± 1.23	9.58 ± 1.89	7.63 ± 2.65	6.99 ± 1.69	10.46 ± 2.09
3T3							
TNFα	5.38 ± 1.56	48.12 ± 8.89*	6.43 ± 0.95	8.34 ± 2.95	9.63 ± 3.82	6.66 ± 2.63	9.61 ± 3.09
IL-1β	2.59 ± 0.96	12.54 ± 3.25*	2.04 ± 1.02	1.02 ± 0.54	1.48 ± 0.54	1.4 ± 0.82	1.17 ± 1.05
IL-6	4.87 ± 1.02	10.02 ± 2.72*	1.35 ± 0.63	6.82 ± 1.58	4.12 ± 0.95	5.8 ± 1.08	5.28 ± 1.56
IL-8	6.25 ± 2.51	17.23 ± 1.65*	7.84 ± 1.25	8.14 ± 0.97	8.52 ± 1.42	7.79 ± 1.27	8.14 ± 2.08
IL-10	15.43 ± 2.01	66.75 ± 6.33*	18.63 ± 5.88	31.15 ± 6.1*	34.78 ± 4.1*	27.51 ± 3.21*	29.71 ± 3.54*

MNS: micro/nanosphere; MNS_RP: retinyl palmitate–loaded micro/nanospheres; MNC_DSW: Dead Sea Water–loaded micro/nanocapsules; TNF: tumor necrosis factor; IL: interleukin; SD: standard deviation; ANOVA: analysis of variance. Values are expressed as the mean of pg/mL of cytokine ± SD analyzed in HaCaT and BALB/3T3 cell line. One-factor ANOVA was performed.
*$p < 0.05$ with respect to control cell cultures.

cultures. These results suggest an active release of anti-inflammatory molecules by fibroblast cells that could benefit the surrounding skin cell types after an exposure to nanoparticulate systems on skin.

Intracellular ROS are natural byproducts of the normal metabolism of oxygen and have important roles in cell signaling and homeostasis.[49] High levels of ROS have damaging effects on cell viability and, in turn, stimulate innate immune responses. According to our flow cytometry analysis, the fraction of H_2DCFDA-positive cells (Figure 4(c) and (d)) treated with MNS, MNS_RP, and MNC_DSW with concentrations of 0.1 and 0.5 mg/mL was similar to the control cultures in both BALB/3T3 and HaCaT cell lines. In contrast, in cell cultures incubated with tert-butyl hydroperoxide, the percentage of H_2DCFDA-positive cells was significantly increased in all cell lines. The absence of ROS production corroborates the low inflammation response that was observed after MNS, MNS_RP, and MNC_DSW incubation in both cell lines.

Genotoxicity studies with Ames test. The cytotoxicity and mutagenic nature of the particles was studied with Ames test (the reverse mutation test on *S. typhimurium*). This method follows the "OECD Guideline for testing of chemicals" Protocol No. 471. Here, the cytotoxicity was assessed by visually inspecting the plates for any inhibition of growth over the bacterial lawn. Genotoxicity was assessed for each strain by calculating the Mutation Index (MI) number as

$$MI = (\text{Number of mutants in sample}/\text{Number of mutants in control})$$

The following assessment criteria were applied: $MI < 1.5$ (non-mutagenic), $1.5 < MI < 2$ (weakly mutagenic), and $MI > 2$ (mutagenic). The mean MI values for the particles tested in the presence of a liver fraction with and without S9 were found to be 0.8 ± 0.3 and 1.1 ± 0.3, respectively. Our data indicates that the developed nanoparticles were not genotoxic under the conditions of the study.

Uptake of MNS_NR by Saos 2 cells. A signicant amount of MNS_NR particles were taken up by Saos 2 cells in 24 h treatment. The actin cytoskeleton was stained green with FITC-labeled

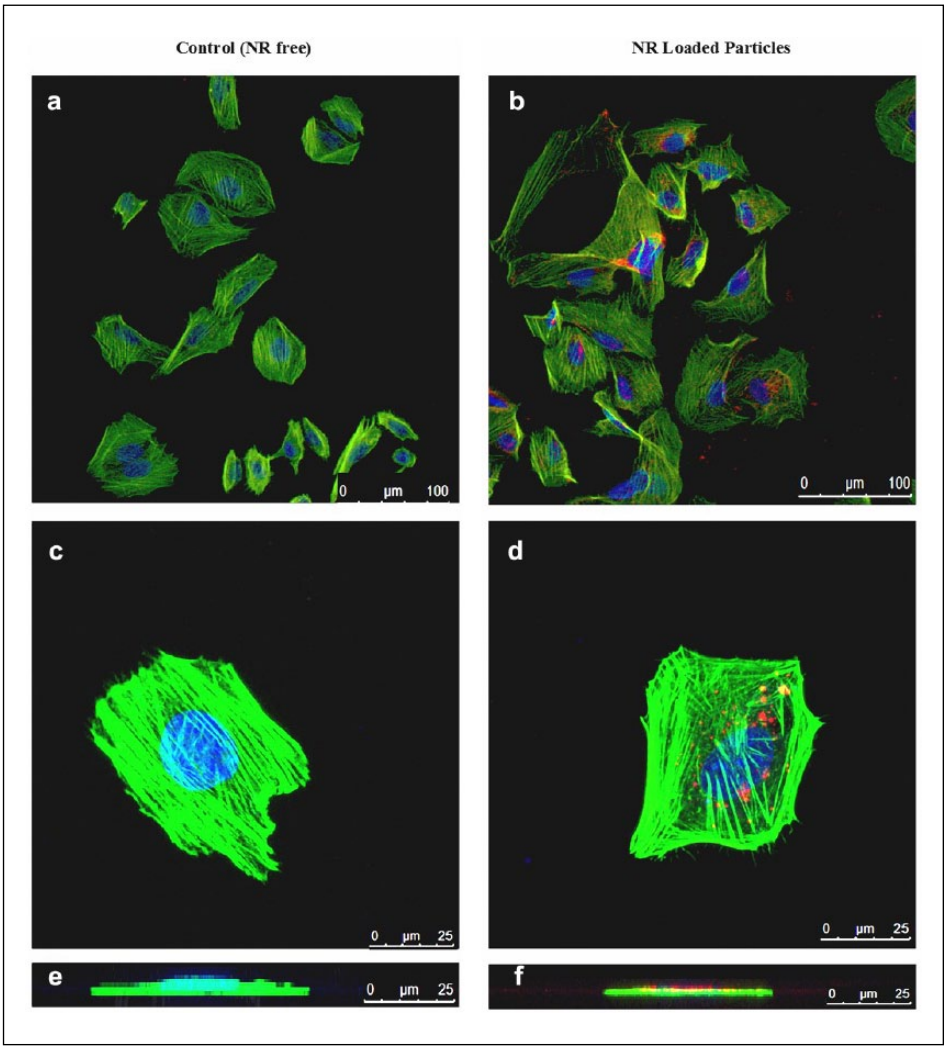

Figure 5. Confocal microscopy (CLSM) images of MNS_NR incubated with Saos 2 cells for 24 h: (a) cells without MNS (control) (20×), (b) MNS_NR after 24 h of culture (20×), (c) cells without MNS (control) (63×), (d) MNS_NR after 24 h of culture (63×), (e) z-stack image of (c), and (f) z-stack image of (d). Spheres were located near the nucleus. Cells were stained with FITC-labeled phalloidin and Draq5 for the cell cytoskeleton (green) and the cell nuclei (blue), respectively. z-Stack images of Saos 2 cells show particle presence in the cells.

phalloidin and cell nucleus blue with Draq5. The cells were then observed with CLSM where MNS_NR were visible as specks in the cytoplasm and near the nuclei (Figure 5(b), (d), (e) and (f)). The particle-free controls (Figure 5(a) and (c)) showed no such specks. Thus, it was shown that the nanoparticles could cross the cell membrane but not the nuclear membrane.

Quantitative analysis of the particles taken up by the cells was studied by measuring Nile Red fluorescence intensity. Cytoskeleton of the Saos 2 cells was separated from the nuclei and Nile Red intensity in the cytoplasm was determined as 4.6 ± 1.2% of the input value.

Transfer of MNP across membranes depends on the particle size. In our previous study, we showed that particles larger than 2 μm could not cross into the cell, but low (166 nm) and mid (426 nm) nano-sized particles could, and generally they accumulated near the nuclei.[10]

Penetration studies in human skin. Human skin samples were used for skin penetration studies and MNS_RPs were applied on the upper layer of the skin samples in the presence of a penetration enhancer, PVA. Epidermis was exposed to air and dermis was immersed in PBS. As expected, no RP could be detected in PBS. RP amount in the skin was determined as 1.2 ± 0.4% and 6.4 ± 1.5% in the presence and absence of stratum corneum (when the stratum corneum was removed), respectively. This was in accordance with the literature; for CdSe quantum dot–loaded PEG particles, penetration increased by 4-fold when the SKH-1 hairless mouse skin was abraded.[20] It is also reported that FITC-conjugated polystyrene nanospheres dispersed in an aqueous gel were clearly visualized within pilosebaceous structures of full-thickness hairless rat and human skin after 2 h of passive permeation. In vivo skin penetration studies also showed that 4 h of PHBV sphere application on the dorsal region of BALB/c mice was adequate for particles to penetrate through the skin and the amount of particles decreased for 10 days after application.[10,50] Therefore, it can be stated that less than 24 h is sufficient for skin penetration of the polymeric materials.

Conclusion

In this study, MNPs of PHBV were prepared for use as drug carriers in the treatment of various skin diseases. RP and DSW were used as model drugs. For certain diseases, specific drugs could be encapsulated in MNPs to achieve optimum healing because of the patient-specific approach. In this context, systems developed in this study have the potential to become personalized treatment tools for the topical administration of vitamin A derivatives. This could be generalized to load hydrophilic and hydrophobic drugs in capsules and spheres, respectively. The PHBV MNPs were shown to penetrate the cell membrane as well as human skin. They can be highly effective without causing any damage due to accumulation, because these particles are biodegradable and would be hydrolyzed at a rate selected by the designer of the carrier. The in vitro evaluation of the particles indicates appropriate cytocompatibility and hemocompatibility, and it can be concluded that these carriers have a significant potential as topical drug delivery systems in the personalized treatment of skin diseases.

Acknowledgements

The authors acknowledge A. Buyuksungur for his significant contribution in the microscopical studies.

Declaration of conflicting interests

The authors declare no potential conflicts of interest with respect to the research, authorship, and/or publication of this article.

Funding

The research was performed within the framework of the FP7-NMP "SkinTreat" project theme under grant agreement no. 213202-2. The authors also acknowledge the support of METU through the project BAP-07-02-2012-101-91.

References

1. Prausnitz MR and Langer R. Transdermal drug delivery. *Nat Biotechnol* 2008; 26(11): 1261–1268.
2. Sloan KB, Wasdo SC and Rautio J. Design for optimized topical delivery: prodrugs and

a paradigm change. *Pharm Res* 2006; 23(12): 2729–2747.
3. Martins IM, Barreiro MF, Coelho M, et al. Microencapsulation of essential oils with biodegradable polymeric carriers for cosmetic applications. *Chem Eng J* 2014; 245: 191–200.
4. David RB. General pharmacology. In: Krieg T, Bickers D and Miyachi Y (eds) *Therapy of skin diseases*. Berlin, Heidelberg: Springer, 2010, vol. 3, pp. 21–27.
5. Barry BW. Novel mechanisms and devices to enable successful transdermal drug delivery. *Eur J Pharm Sci* 2001; 14(2): 101–114.
6. Venuganti VVK and Perumal OP. Poly(amidoamine) dendrimers as skin penetration enhancers: influence of charge, generation, and concentration. *J Pharm Sci* 2009; 98(7): 2345–2356.
7. Arora A, Prausnitz MR and Mitragotri S. Microscale devices for transdermal drug delivery. *Int J Pharm* 2008; 364(2): 227–236.
8. Pereira VH, Salgado AJ, Oliveira JM, et al. In vivo biodistribution of carboxymethylchitosan/poly(amidoamine) dendrimer nanoparticles in rats. *J Bioact Compat Polym* 2015; 26(6): 619–627.
9. Hasirci V and Yucel D. Polymers used in tissue engineering. *Encycl Biomater Biomed Eng* 2007; 1(1): 1–17.
10. Eke G, Kuzmina AM, Goreva AV, et al. In vitro and transdermal penetration of PHBV micro/nanoparticles. *J Mater Sci Mater Med* 2014; 25(6): 1471–1481.
11. Aydemir-Sezer U, Arslantunali D, Aksoy AE, et al. Poly (ε-caprolactone) composite scaffolds loaded with gentamicin-containing β-tricalcium phosphate/gelatin microspheres for bone tissue engineering applications. *J Appl Polym Sci* 2014; 131(8): 1–11.
12. Baroli B. Penetration of nanoparticles and nanomaterials in the skin: fiction or reality? *J Pharm Sci* 2010; 99(1): 21–50.
13. Yu W, Bien-Aime S, Li L, et al. Injectable microspheres for extended delivery of bioactive insulin and salicylic acid. *J Bioact Compat Polym* 2015; 30(3): 340–346.
14. Maria NS, Barnes SR, Jacobs RE, et al. In vivo monitoring of natural killer cell trafficking during tumor immunotherapy. *Magn Reson Insights* 2014; 7: 15–21.
15. Endo M, Yang Y and Sugiyama H. DNA origami technology for biomaterials applications. *Biomater Sci* 2013; 1(4): 347–360.
16. Yuk SH, Oh KS, Park J, et al. Docetaxel-loaded composite nanoparticles formed by a temperature-induced phase transition for cancer therapy. *J Bioact Compat Polym* 2012; 27(5): 441–452.
17. Oliver JC. Drug transport to brain with targeted nanoparticles. *NeuroRx* 2005; 2(1): 108–119.
18. Kim H, Kim B, Kim H, et al. Synthesis and in vitro biological activity of retinyl retinoate, a novel hybrid retinoid derivative. *Bioorg Med Chem* 2008; 16(12): 6387–6393.
19. Sachs DL and Voorhees JJ. Vitamin A: retinoids and the treatment of aging skin. In: Farris PK (ed.) *Cosmeceuticals and cosmetic practice*. Chichester: Wiley, 2014, vol. 8, pp. 81–93.
20. Goope NV, Roberts DW, Webb P, et al. Quantitative determination of skin penetration of PEG-coated CdSe quantum dots in dermabraded but not intact SKH-1 hairless mouse skin. *Toxicol Sci* 2009; 111(1): 37–48.
21. Hasirci V, Yilgor P, Endogan T, et al. Polymer fundamentals: polymer synthesis. In: Ducheyne P, Healy K, Hutmacher DE, et al. (eds) *Comprehensive biomaterials*. Amsterdam: Elsevier, 2011, vol. 1, pp. 349–371.
22. Yilgor P, Hasirci N and Hasirci V. Sequential BMP-2/BMP-7 delivery from polyester nanocapsules. *J Biomed Mater Res A* 2010; 93(2): 528–536.
23. Enderle JD and Bronzino JD (eds). *Introduction to biomedical engineering*. Burlington, MA: Academic Press, 2012.
24. Hasirci N. Micro and nano systems in biomedicine and drug delivery. In: Mozafari MR (ed.) *Nanomaterials and nanosystems for biomedical applications*. Dordrecht: Springer, Inc., 2007, pp. 1–26.
25. Gursel I, Korkusuz F, Turesin F, et al. In vivo application of biodegradable controlled antibiotic release systems for the treatment of implant-related osteomyelitis. *Biomaterials* 2000; 22(1): 73–80.
26. Sripriyalakshmi S, Jose P, Ravindran A, et al. Recent trends in drug delivery system using protein nanoparticles. *Cell Biochem Biophys* 2014; 70: 17–26.
27. Errico C, Goñi-de-Cerio F, Alderighi M, et al. Retinyl palmitate–loaded poly(lactide-co-glycolide) nanoparticles for the topical treatment of skin diseases. *J Bioact Compat Polym* 2012; 27(6): 604–620.

28. Halevy S, Giryes H, Friger M, et al. Dead Sea bath salt for the treatment of psoriasis vulgaris: a double-blind controlled study. *J Eur Acad Dermatol Venereol* 1997; 9(3): 237–242.
29. Dessy A, Kubowicz S, Alderighi M, et al. Dead Sea Minerals loaded polymeric nanoparticles. *Colloids Surf B Biointerfaces* 2011; 87(2): 236–242.
30. Kurlandsky SB, Duell EA, Kang S, et al. Auto-regulation of retinoic acid biosynthesis through regulation of retinol esterification in human keratinocytes. *J Biol Chem* 1996; 271(26): 15346–15352.
31. Oliveira MB, Prado AH, Bernegossi J, et al. Topical application of retinyl palmitate-loaded nanotechnology-based drug delivery systems for the treatment of skin aging. *Biomed Res Int* 2014; 2014: 632570.
32. ASTM F756-08:2008.Standard practice for assessment of hemolytic properties of materials.
33. Errico C, Bartoli C, Chiellini F, et al. Poly(hydroxyalkanoates)-based polymeric nanoparticles for drug delivery. *Biomed Res Int* 2009; 10: 1–10.
34. Lalatsa A, Schätzlein AG, Mazza M, et al. Amphiphilic poly (L-amino acids)—new materials for drug delivery. *J Control Release* 2012; 161(2): 523–536.
35. Sane A and Limtrakul J. Formation of retinyl palmitate-loaded poly (l-lactide) nanoparticles using rapid expansion of supercritical solutions into liquid solvents (RESOLV). *J Supercrit Fluids* 2009; 51(2): 230–237.
36. Mendes JBE, Riekes MK, Oliveira VM, et al. PHBV/PCL microparticles for controlled release of resveratrol: physicochemical characterization, antioxidant potential, and effect on hemolysis of human erythrocytes. *Scientific World Journal* 2012; 2012: 542937.
37. Gursel I and Hasirci V. Properties and drug release behaviour of poly(3-hydroxybutyric acid) and various poly(3-hydroxybutyrate-hydroxyvalerate) copolymer microcapsules. *J Microencapsul* 1995; 12(2): 185–193.
38. Qu XH, Wu Q, Zhang KY, et al. In vivo studies of poly(3-hydroxybutyrate-co-3-hydroxyhexanoate) based polymers: biodegradation and tissue reactions. *Biomaterials* 2006; 27(19): 3540–3548.
39. Sevastianov VI, Perova NV, Shishatskaya EI, et al. Production of purified polyhydroxyalkanoates (PHAs) for applications in contact with blood. *J Biomater Sci Polym Ed* 2003; 14(10): 1029–1042.
40. Artsis MI, Bonartsev A, Iordanskii AL, et al. Biodegradation and medical application of microbial poly(3-hydroxybutyrate). *Mol Cryst Liq Cryst* 2012; 555: 232–262.
41. Kim B, Kim JE, Kim H, et al. Co-treatment with retinyl retinoate and a PPARα agonist reduces retinoid dermatitis. *Int J Dermatol* 2012; 51(6): 733–741.
42. Yang Y, Qu Y, Lü X, et al. Global gene expression analysis of the effects of gold nanoparticles on human dermal fibroblasts. *J Biomed Nanotechnol* 2010; 6(3): 234–246.
43. Chen Y, Wan Y, Wang Y, et al. Anticancer efficacy enhancement and attenuation of side effects of doxorubicin with titanium dioxide nanoparticles. *Int J Nanomedicine* 2011; 6: 2321–2326.
44. Cheng LC, Jiang X, Wang J, et al. Nano-bio effects: interaction of nanomaterials with cells. *Nanoscale* 2013; 5(9): 3547–3569.
45. Liu X, Zhu H, Lu HJ, et al. Real-time investigation of engineered nanomaterials cytotoxicity in living alveolar epithelia with hopping probe ion conductance microscopy. *Adv Mater Res* 2013; 651: 24–28.
46. Dinarello CA. Proinflammatory cytokines. *Chest* 2000; 118(2): 503–508.
47. Schanen BC, Karakoti AS, Seal S, et al. Exposure to titanium dioxide nanomaterials provokes inflammation of an in vitro human immune construct. *ACS Nano* 2009; 3(9): 2523–2532.
48. Shachar I and Karin N. The dual roles of inflammatory cytokines and chemokines in the regulation of autoimmune diseases and their clinical implications. *J Leukoc Biol* 2013; 93(1): 51–61.
49. Han D, Williams E and Cadenas E. Mitochondrial respiratory chain-dependent generation of superoxide anion and its release into the intermembrane space. *Biochem J* 2001; 353: 411–416.
50. Jeong YI, Cho CS, Kim SH, et al. Preparation of poly (DL-lactide-co-glycolide) nanoparticles without surfactant. *J Appl Polym Sci* 2001; 80(12): 2228–2236.